Study on Transient Recovery Voltages for Transformer-Limited Faults

Hiroki Ito, *Member, IEEE*, Hiroki Kajino, *Member, IEEE*, Yoshibumi Yamagata, Kenji Kamei, Toshiki Idemaru, and Hiromu Shinkai

***Abstract*—Severe transient recovery voltage (TRV) after current interruption may appear when a fault occurs in the immediate vicinity of a power transformer without any appreciable capacitance between the transformer and the circuit breaker. These faults are called transformer-limited faults (TLFs), that may cause higher rate of rise of TRV than the standard values specified for terminal fault test duties T10 and T30 of IEC 62271-100 and IEEE standard C37.06. TRVs for TLF conditions with large capacity and high-voltage shell-type power transformer were measured by the capacitor current injection method. The impedance frequency response were also measured by the frequency-response analysis (FRA) and then TRVs were reproduced by the simplified transformer model with a series connection of parallel circuit of inductance, capacitance, and resistance evaluated by the FRA measurements. The reproduced TRV showed good agreement with the measured TRV even though deformation from a sinusoidal waveshape was observed due to superposition of higher frequency components on the TRV.**

***Index Terms*—Amplitude factor, circuit breaker (CB), frequency-response analysis (FRA), rate of rise of TRV, transformer-limited fault, transient recovery voltage.**

I. Introduction

LARGE capacity and high-voltage power transformers, such as 525/275 kV-1500 MVA and 1050/525 kV-3000 MVA classes, capable of onsite assembly, were developed to meet a network requirement for high-capacity power delivery. For this purpose, the transformers were developed to reduce the number of legs (iron cores) and coil groups in order to realize compact and reduced weight designs. The requirement for a compact design may reduce the equivalent surge capacitance of the transformer, resulting in a more severe transient recovery voltage (TRV) in transformer-limited fault (TLF) duty for a circuit breaker (CB) than the specified values for terminal fault test duties T10 and T30 in the IEC 62271-100 standard and IEEE standard C37.06, especially for the CB connected directly to the primary or secondary or tertiary winding of the transformer.

Manuscript received September 01, 2013; revised November 08, 2013; accepted February 03, 2014. Paper no. TPWRD-01011-2013.

H. Ito and H. Kajino are with Mitsubishi Electric Corp., T&D Systems Center, Tokyo 100-8310, Japan (e-mail: ito.hiroki@aj.mitsubishielectric.co.jp; kajino.hiroki@bx.MitsubishiElectric.co.jp).

Y. Yamagata is with Takaoka Electric Manufacturing Company, Tochigi 323-0806, Japan (e-mail: yoshibumi_yamagata@notes.takaoka.co.jp).

K. Kamei is with Mitsubishi Electric Corp., T&D Systems Center, Hyogo 661-8661, Japan (e-mail: Kamei.Kenji@ce.MitsubishiElectric.co.jp).

T. Idemaru and H. Shinka are with Mitsubishi Electric Corp., T&D Systems Center, Hyogo 678-0256, Japan (e-mail: Idemaru.Toshiki@dw.MitsubishiElectric.co.jp; Shinkai.Hiromu@cb.MitsubishiElectric.co.jp).

Color versions of one or more of the figures in this paper are available online at http://ieeexplore.ieee.org.

Digital Object Identifier 10.1109/TPWRD.2014.2304968

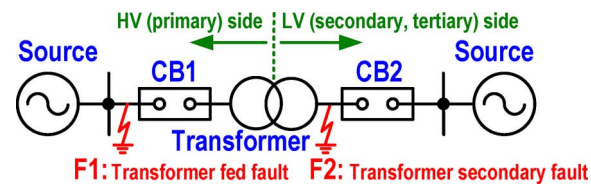

Fig. 1. Transformer-limited faults (TLFs).

In accordance with IEC SC 17A requests, CIGRE Working Group A3.22 investigated TRV for TLF conditions based on available technical specifications and recommended higher rate of rise of TRV (RRRV) and shorter time to the TRV peak than the existing IEC standard values for 1100/1200-kV CBs [1], [2]. The recommendation was determined by the transformer impedance and its equivalent surge capacitance of a 1100-kV power transformer (specified as 9 nF).

Recently, a transformer model for TRV analysis was reported [3]–[5], but there are not enough actual survey results, and it is thought that examination is more necessary [6], [7]. TRVs for TLF conditions with the primary, secondary, and tertiary sides of 525-kV–1500-MVA shell-type transformer were measured by a capacitor current injection method. Impedance frequency responses from the primary, secondary, and tertiary windings of the transformer were also measured by frequency-response analysis (FRA).

A simplified transformer model with a series connection of parallel circuits with capacitance (C), inductance (L), and resistance (R) was estimated based on the FRA measurements corresponding to the number of resonant frequencies. Then, TRVs were reproduced by the simplified transformer model. The comparison between the measured TRVs and the reproduced TRVs provides detailed technical information on switching phenomena related to TLF conditions.

II. TRV for TLFs

As shown in Fig. 1, TLF covers two types of faults for CB1: transformer fed fault and transformer secondary fault depending on a fault location either on the opposite (F1 point at HV) side or the same side of the transformer (F2 point at LV).

The TRV frequency is generally determined by the inductance (L) and the equivalent surge capacitance (C) of the transformer.

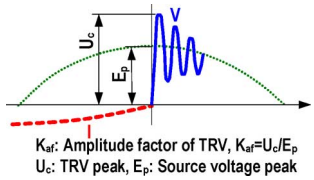

Fig. 2. TRV for TLF conditions.

Fig. 3. The 1500-MVA shell-type three-phase transformer.

TABLE I
SPECIFICATION OF THE 1500-MVA SHELL-TYPE TRANSFORMER

Rated voltage	Primary	525 kV / $\sqrt{3}$
	Secondary	275 kV / $\sqrt{3}$
	Tertiary	63 kV
Rated capacity	Primary / Secondary	1500 MVA
	Tertiary	450 MVA
Short-circuit Impedance (measured values, based on 1500 MVA)	Primary - Secondary	13.8 %
	Primary - Tertiary	70.3 %
	Secondary - Tertiary	44.8 %

It ranges from several kilohertz to several ten kilohertz depending on these parameters. In such cases, the rate of rise of trv (RRRV) may exceed the values specified in the standards for terminal fault test duties T10 and T30.

Fig. 3 shows a photograph of the 525-kV–1500-MVA shell-type autotransformer used for TRV measurements and Table I summarizes its specification for primary, secondary, and tertiary windings (see Table I).

III. TRV MEASUREMENTS FOR TLF CONDITIONS

A. TRV Measurement by the Capacitor Current Injection Method

Fig. 4 shows a TRV measurement circuit using the capacitor current injection method according to Annex F of IEC 62271-100. This circuit is assumed for first pole to clear of the 3LG condition. When TRV for fault clearing on the primary side was measured in the circuit, a tertiary terminal (63 kV) was ungrounded, a secondary terminal (275 kV) was grounded, and a primary terminal (525 kV) was connected to a capacitor with several 100 μF, which can supply an oscillating current with a frequency determined by the capacitance and the transformer inductance. The voltage at the primary terminal was measured

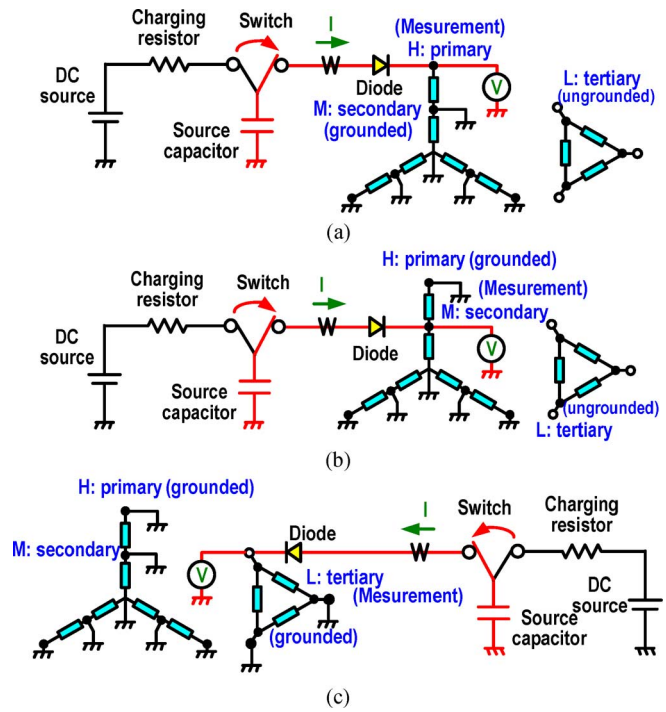

Fig. 4. Capacitor current injection method in IEC 62271-100. (a) Measuring circuit for the primary side. (b) Measuring circuit for the secondary side. (c) Measuring circuit for the tertiary side.

with a high-voltage divider after a diode interrupted the current. Similarly, the voltages at the secondary and tertiary terminals were also measured by changing the grounding and the ungrounded points.

Typical TRV waveforms measured by capacitor-current injection are shown in Fig. 5. The TRV for the primary side shows a sinusoidal shape waveform. On the other hand, TRVs for the secondary and tertiary sides show a slight deformation from a sinusoidal shape due to superimposition of higher frequency components than a main TRV frequency. The effect of the polarity of the charged capacitor as well as the direction of the diode on TRV was checked and it was confirmed that there were no significant differences of these impacts on TRVs.

The TRV frequency and amplitude factor obtained from the measured TRVs for the primary, secondary, and tertiary sides are summarized in Table II. The amplitude factor of TRV for the secondary side is reduced compared with TRVs for the primary and tertiary sides due to waveform deformation. It should be noted that the amplitude factors do not exceed the standard value of 1.7.

B. Impedance Frequency Responses by FRA Measurements

FRA measurements are usually applied to investigate internal frequency resonance in relation to dielectric stress or to detect any deviations from the response of a particular transformer. The information on multiple frequency responses from a transformer can also provide a simplified transient transformer model with a series connection of multiple parallel circuits of L, C, and R.

Typical responses obtained by FRA measurements with the first pole to clear at the primary, secondary, and tertiary sides

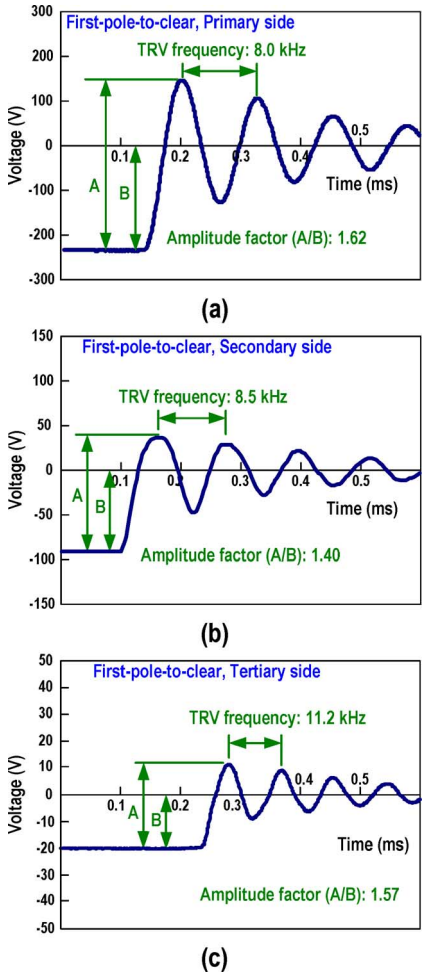

Fig. 5. TRV measurements by the capacitor current injection method. (a) TRV for the primary side. (b) TRV for the secondary side. (c) TRV for the tertiary side.

TABLE II
TRV FREQUENCY AND AMPLITUDE FACTOR

TRV	Primary	Secondary	Tertiary
Frequency	8.0 kHz	8.5 kHz	11.2 kHz
Amplitude factor	1.62	1.40	1.57

of a 1500-MVA shell-type transformer are shown in Fig. 6. The same circuit as that used for the TRV measurements was used for the FRA measurements.

The prominent resonance frequency of the impedance frequency response from the primary side is 7.9 kHz. The impedance frequency response from the secondary side shows two resonance frequencies at 8.04 kHz and 15.5 kHz. Furthermore, the impedance frequency response from the tertiary side shows three resonance frequencies at 11.1, 16.8, and 24.5 kHz. This appearance of multiple resonance frequencies can deform the TRV waveforms.

IV. TRV REPRODUCTION USING THE SIMPLIFIED TRASFORMER MODEL BASED ON FRA MEASUREMENT

TRV waveforms can be reproduced by a simplified transformer model with a series connection of multiple parallel circuits of L, C, and R based on the FRA measurements and/or a

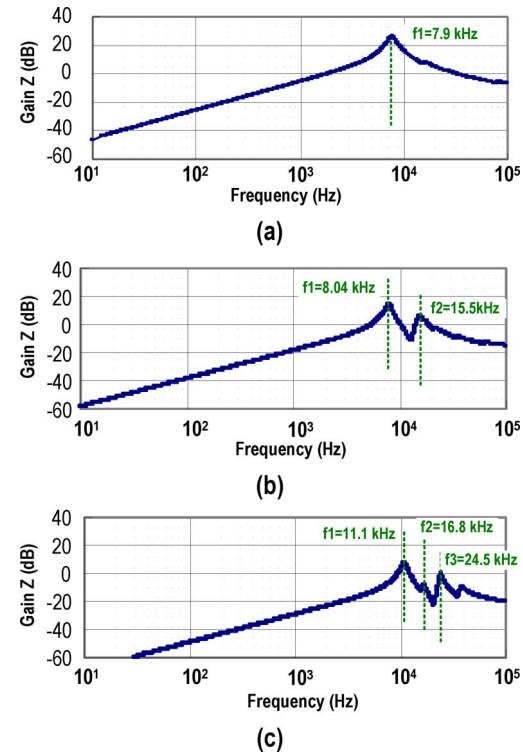

Fig. 6. Frequency response by FRA measurements with a 1500-MVA shell-type transformer. (a) Frequency response for the primary side. (b) Frequency response for the secondary side. (c) Frequency response for the tertiary side.

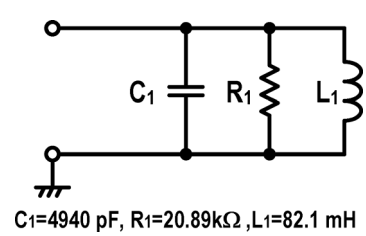

Fig. 7. Simplified transformer model for the primary side.

manufacturer model based on the transformer design. In the case of the simplified transformer model, these equivalent lumped L, C, and R parameter circuits can be evaluated from a linear-fitted slope of the gain and/or gain at these resonant points. Typical evaluation will be explained.

A. TRV Reproduction for the Primary Side of the Transformer

The simplified transformer model for the primary side can be provided with a single set of parallel-connected L, C and R circuits as shown in Fig. 7, since the impedance frequency response shown in Fig. 6(a) has one prominent resonance point.

The impedance Z_{in} and the impedance gain G_{ain} can be expressed with L_1, C_1, and R_1 by

$$Zin = \frac{\frac{\omega^2 {L_1}^2}{R_1} + j\omega L_1(1-\omega^2 L_1 C_1)}{\omega^4 {L_1}^2 {C_1}^2 + \omega^2\left(\frac{{L_1}^2}{{R_1}^2} - 2L_1C_1\right) + 1} \quad (1)$$

$$Gain = 20\log|Zin|. \quad (2)$$

The resonant angular frequency ω_0 can be given by

$$\omega_1 = 2\pi f_1 = \frac{1}{\sqrt{\mathrm{L_1 C_1}}}, f_1 = \frac{1}{(2\pi\sqrt{\mathrm{L_1 C_1}})}. \quad (3)$$

Substituting (3) into (1), gain is expressed by

$$\mathrm{Zin}\,(\omega_1) = \mathrm{R_1}. \quad (4)$$

Therefore, the resistance $\mathrm{R_1}$ can be evaluated from the gain (26.4 dB) at the resonance frequency

$$\mathrm{Zin} = \mathrm{R_1} = 10^{26.4\ \mathrm{dB}/20} = 20.89\ \mathrm{k\Omega}. \quad (5)$$

When the frequency is much smaller than the resonant frequency ($\mathrm{f} \ll \mathrm{f_0}$), $\omega\mathrm{C}$ approaches zero. It is also assumed that $\omega\mathrm{L_1} \ll \mathrm{R_1}$, therefore

$$\mathrm{Zin}(f \ll f_1) \approx \frac{\frac{\omega^2 \mathrm{L_1}^2}{\mathrm{R_1}} + j\omega\mathrm{L_1}}{1 + \frac{\omega^2 \mathrm{L_1}^2}{\mathrm{R_1}}} \approx j\omega\mathrm{L_1}. \quad (6)$$

On the contrary, when the frequency is much larger than the resonant frequency ($\mathrm{f} \gg \mathrm{f_0}$), $\omega\mathrm{L}$ approaches infinity. It is also assumed that $1/\omega\mathrm{C_1} \ll \mathrm{R_1 l}$; therefore

$$\mathrm{Zin}\,(f \gg f_1) \approx \frac{\frac{1}{\omega \mathrm{C_1 R_1}} - j}{\frac{1}{\omega \mathrm{C_1 R_1}^2} + \omega\mathrm{C_1}} \approx \frac{1}{j\omega\mathrm{C_1}}. \quad (7)$$

The impedance gain linearly increases with the frequency in the ranges from 10 to several kilohertz (up to the resonant point) so the slope of the gain can provide the equivalent inductance $\mathrm{L_1}$ or it can also be evaluated from a gain of -5.75 dB at the frequency 1 kHz according to (6)

$$\mathrm{L_1} = 10^{-5.75\ \mathrm{dB}/20} \times 10^3 \times \frac{10^3}{2\pi \times 1\ \mathrm{kHz} \times 10^3} = 82.1\ \mathrm{mH}. \quad (8)$$

On the other hand, the impedance gain can linearly decrease with the frequency higher than the resonant point so the slope of the gain can provide an inverse value of the equivalent capacitance $\mathrm{C_1}$ or it can be evaluated from a gain of -0.97 dB at the frequency of 30 kHz

$$\mathrm{C_1} = \frac{10^{12}}{10^{-0.62\ \mathrm{dB}/20} \times 10^3 \times 2\pi \times 30\ \mathrm{kHz} \times 10^3} = 4940\ \mathrm{pF}. \quad (9)$$

Accordingly, the simplified transformer model for the primary side can be obtained by the response of the FRA measurement. The impedance response evaluated with the simplified transformer model agreed with the FRA measurement well (see Fig. 8).

These equivalent circuit parameters can be deduced with a dumping oscillating response to the step voltage assuming a single frequency by the second Kyoto University method [2]. Fig. 9 shows a measured waveform. The equivalent capacitance of 5240 pF as well as the equivalent inductance and resistance obtained by the method agrees well with the values evaluated by the FRA measurement.

The TRV for the primary side was calculated with the simplified transformer model and compared with the measured TRV by the capacitor current injection method shown in Fig. 10. TRV reproduced by the simplified transformer model shows good agreement with the measurements.

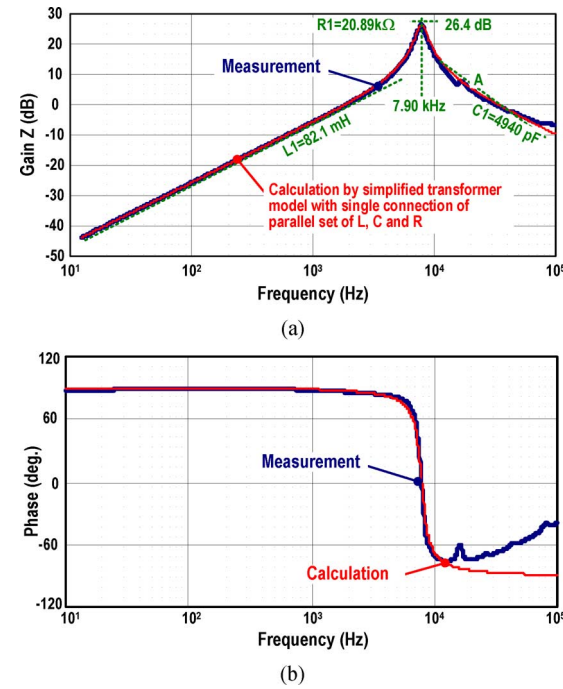

Fig. 8. Response by the simplified transformer model. (a) Gain. (b) Phase.

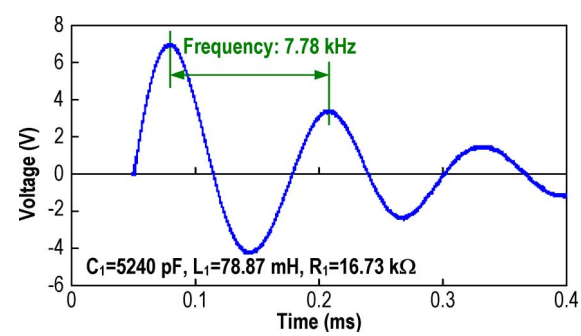

Fig. 9. Damped oscillation response by the second Kyoto university method.

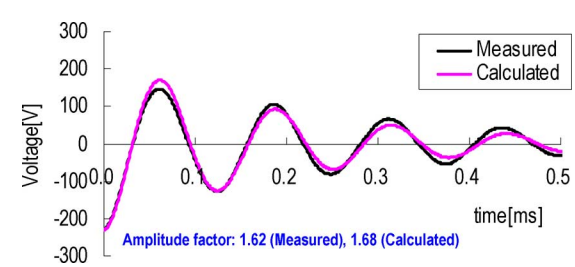

Fig. 10. TRV reproduced by the simplified transformer model.

The TRV waveform shown in Fig. 10 can be expressed as follows. Here, $\mathrm{V_o}$ is a voltage across the CB at the current zero

$$\mathrm{v(t)} = \mathrm{V_0} e^{-\mathrm{t}/2\mathrm{R_1 C_1}} \left(\cos\left(2\pi f_1 - \mathrm{t}\right) - \frac{\sin(2\pi f_1 - t)}{4\pi f_1 \mathrm{R_1 C_1}} \right) \quad (10)$$

$$f_1 = \frac{1}{2\pi}\sqrt{\frac{1}{\mathrm{L_1 C_1}} - \frac{1}{(2\mathrm{R_1 C_1})^2}}. \quad (11)$$

B. TRV Reproduction for the Secondary Side of the Transformer

The impedance response from the secondary side shows two prominent resonance frequencies at 8.04 and 15.5 kHz. It means that the simplified transformer model has a series connection of two set of parallel circuits of L_1, L_2, C_1, C_2, R_1, and R_2. The impedance Z_{in} can be provided by

$$\mathrm{Zin} = \frac{\frac{\omega^2 {L_1}^2}{R_1} + j\omega L_1(1-\omega^2 L_1 C_1)}{\omega^4 {L_1}^2 {C_1}^2 + \omega^2\left(\frac{{L_1}^2}{{R_1}^2} - 2L_1C_1\right) + 1} + \frac{\frac{\omega^2 {L_2}^2}{R_2} + j\omega L_2(1-\omega^2 L_2 C_2)}{\omega^4 {L_2}^2 {C_2}^2 + \omega^2\left(\frac{{L_2}^2}{{R_2}^2} - 2L_2C_2\right) + 1}. \quad (12)$$

Equation (12) confirms that its two sets of addition are of the same form as (1). Therefore, L_1, L_2, C_1, C_2, R_1, and R_2 can be derived in procedure the same as (3)–(8).

The impedance gain linearly increases with the frequency in the ranges from 10 to several kilohertz (up to the first resonant point) so the equivalent total inductance $L = L_1 + L_2$ can be evaluated from the gain of $-$ 18.95 dB at the frequency 1 kHz.

$$L_1 + L_2 = 10^{-18.95\ \mathrm{dB}/20} \times 10^3 \times \frac{10^3}{2\pi \times 1\ \mathrm{kHz} \times 10^3} = 17.96\ \mathrm{mH}. \quad (13)$$

On the other hand, the impedance gain linearly decreases with the frequency higher than the second resonant point so the total capacitance $C = 1(1/C_1 + 1/C_2)$ can be evaluated from a gain of -14.03 dB at the frequency 60 kHz

$$\frac{1}{\frac{1}{C_1} + \frac{1}{C_2}} = \frac{10^{12}}{10^{-14.03\ \mathrm{dB}/20} \times 10^3 \times 2\pi \times 60\ \mathrm{kHz} \times 10^3} = 13340\ \mathrm{pF}. \quad (14)$$

Each resonant frequency provides the following equations:

$$f_1 = \frac{1}{(2\pi\sqrt{L_1C_1})} = 8.04\ \mathrm{kHz} \quad (15)$$

$$f_2 = \frac{1}{(2\pi\sqrt{L_2C_2})} = 15.5\ \mathrm{kHz}. \quad (16)$$

The resistances R_1 and R_2 can be evaluated from gains (14.14 and 5.89 dB) at each resonance frequency

$$R_1 = 10^{14.14\ \mathrm{dB}/20} = 5.09\ \mathrm{k\Omega} \quad (17)$$

$$R_2 = 10^{5.89\ \mathrm{dB}/20} = 1.97\ \mathrm{k\Omega}. \quad (18)$$

Similarly, the simplified transformer model for the secondary side can be obtained by the response of the FRA measurement as shown in Fig. 11. The impedance response evaluated with the simplified transformer model agreed with the FRA measurement well (see Fig. 12).

The TRV for the secondary side was calculated with the simplified transformer model and compared with the measured TRV

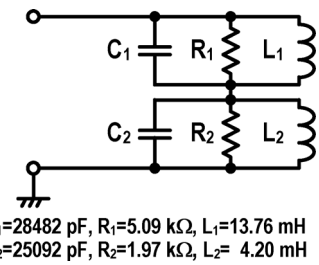

Fig. 11. Simplified transformer model for the secondary side.

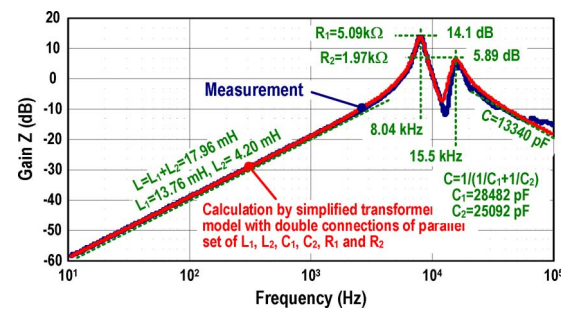

Fig. 12. Response by the simplified transformer model.

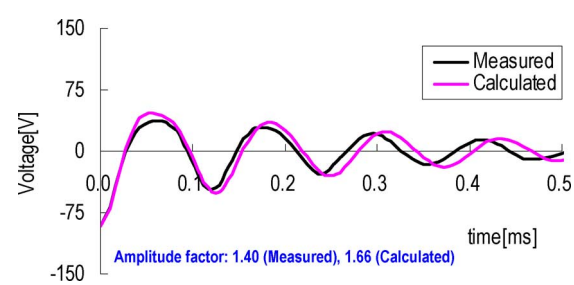

Fig. 13. TRV reproduced by the simplified transformer model.

by the capacitor current injection method shown in Fig. 13. TRV reproduced by the simplified transformer model shows good agreement with the measurements, even though it exhibits some deformation due to double frequency components.

The TRV waveform shown in Fig. 13 can be expressed as follows. Here, V_o is a voltage across the CB at the current zero

$$\mathrm{v(t)} = \frac{L_1}{L_1+L_2} V_0 e^{-t/2R_1C_1} \cdot \left(\cos(2\pi f_1 - t) - \frac{\sin(2\pi f_1 - t)}{4\pi f_1 R_1 C_1}\right) + \frac{L_2}{L_1+L_2} V_0 e^{-t/2R_2C_2} \cdot \left(\cos(2\pi f_2 - t) - \frac{\sin(2\pi f_2 - t)}{4\pi f_2 R_2 C_2}\right) \quad (19)$$

$$f_1 = \frac{1}{2\pi}\sqrt{\frac{1}{L_1C_1} - \frac{1}{(2R_1C_1)^2}},$$

$$f_2 = \frac{1}{2\pi}\sqrt{\frac{1}{L_2C_2} - \frac{1}{(2R_2C_2)^2}}. \quad (20)$$

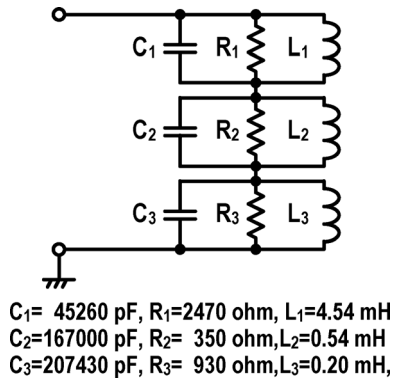

Fig. 14. Simplified transformer model for the tertiary side.

C. TRV Reproduction for Tertiary Side of the Transformer

The impedance response from the tertiary side shows three prominent resonance frequencies at 11.1, 16.8, and 24.5 kHz. It means that the simplified transformer model has a series connection of three set of parallel circuits of L_1, L_2, L_3, C_1, C_2, C_3, R_1, R_2, and R_3. The impedance Z_{in} can be provided by

$$\begin{aligned} \mathrm{Zin} = & \frac{\frac{\omega^2 {L_1}^2}{R_1} + j\omega L_1(1-\omega^2 L_1 C_1)}{\omega^4 {L_1}^2 {C_1}^2 + \omega^2\left(\frac{{L_1}^2}{{R_1}^2} - 2L_1C_1\right) + 1} \\ & + \frac{\frac{\omega^2 {L_2}^2}{R_2} + j\omega L_2(1-\omega^2 L_2 C_2)}{\omega^4 {L_2}^2 {C_2}^2 + \omega^2\left(\frac{{L_2}^2}{{R_2}^2} - 2L_2C_2\right) + 1} \\ & + \frac{\frac{\omega^2 {L_3}^2}{R_3} + j\omega L_3(1-\omega^2 L_3 C_3)}{\omega^4 {L_3}^2 {C_3}^2 + \omega^2\left(\frac{{L_3}^2}{{R_3}^2} - 2L_3C_3\right) + 1}. \end{aligned} \quad (21)$$

Each resonant frequency provides the following equations:

$$f_1 = \frac{1}{(2\pi\sqrt{L_1C_1})} = 11.1 \text{ kHz} \quad (22)$$

$$f_2 = \frac{1}{(2\pi\sqrt{L_2C_2})} = 16.8 \text{ kHz} \quad (23)$$

$$f_3 = \frac{1}{(2\pi\sqrt{L_3C_3})} = 24.5 \text{ kHz}. \quad (24)$$

The resistances R_1, R_2, and R_3 can be evaluated from gains (7.84, -9.16, and 0.65 dB) at each resonance frequency

$$R_1 = 10^{7.84 \text{ dB}/20} = 2.47 \text{ k}\Omega \quad (25)$$

$$R_2 = 10^{-9.16 \text{ dB}/20} = 0.35 \text{ k}\Omega \quad (26)$$

$$R_3 = 10^{0.65 \text{ dB}/20} = 0.93 \text{ k}\Omega. \quad (27)$$

Similarly, the simplified transformer model for the tertiary side can be obtained by the response of the FRA measurement as shown in Fig. 14. The impedance response evaluated with the simplified transformer model agreed with the FRA measurement well.

The TRV for the tertiary side was calculated with the simplified transformer model and compared with the measured TRV by the capacitor current injection method shown in Fig. 16. TRV

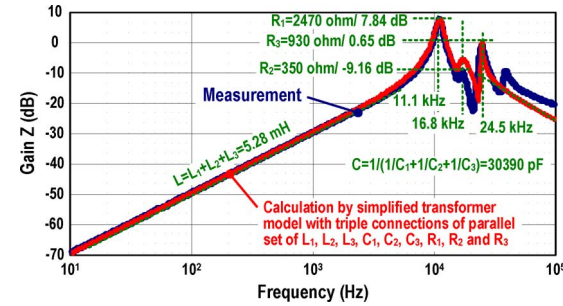

Fig. 15. Response by the simplified transformer model.

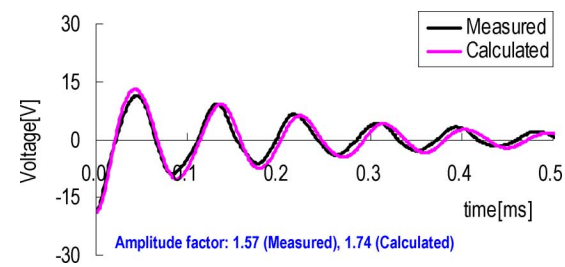

Fig. 16. TRV reproduced by the simplified transformer model.

reproduced by the simplified transformer model shows good agreement with the measurements, even though it exhibits some deformation due to triple frequency components.

The TRV waveform shown in Fig. 16 can be expressed as follows. Here, V_o is a voltage across the CB at the current zero

$$\begin{aligned} v(t) = & \frac{L_1}{L_1+L_2+L_3} V_0 e^{-t/2R_1C_1} \\ & \cdot \left(\cos(2\pi f_1 - t) - \frac{\sin(2\pi f_1 - t)}{4\pi f_1 R_1 C_1}\right) \\ & + \frac{L_2}{L_1+L_2+L_3} V_0 e^{-t/2R_2C_2} \\ & \cdot \left(\cos(2\pi f_2 - t) - \frac{\sin(2\pi f_2 - t)}{4\pi f_2 R_2 C_2}\right) \\ & + \frac{L_3}{L_1+L_2+L_3} V_0 e^{-t/2R_3C_3} \\ & \cdot \left(\cos(2\pi f_3 - t) - \frac{\sin(2\pi f_3 - t)}{4\pi f_3 R_3 C_3}\right) \end{aligned} \quad (28)$$

$$\begin{aligned} f_1 &= \frac{1}{2\pi}\sqrt{\frac{1}{L_1C_1} - \frac{1}{(2R_1C_1)^2}}, \\ f_2 &= \frac{1}{2\pi}\sqrt{\frac{1}{L_2C_2} - \frac{1}{(2R_2C_2)^2}}, \\ f_3 &= \frac{1}{2\pi}\sqrt{\frac{1}{L_3C_3} - \frac{1}{(2R_3C_3)^2}}. \end{aligned} \quad (29)$$

The simulation can also explain the TRV amplitude factor, which is reduced to less than 2.0 without considering any losses due to a distributed parameter circuit (inductance and capacitance) characteristic on a practical transformer resulting in a TRV synthesized with plural frequencies.

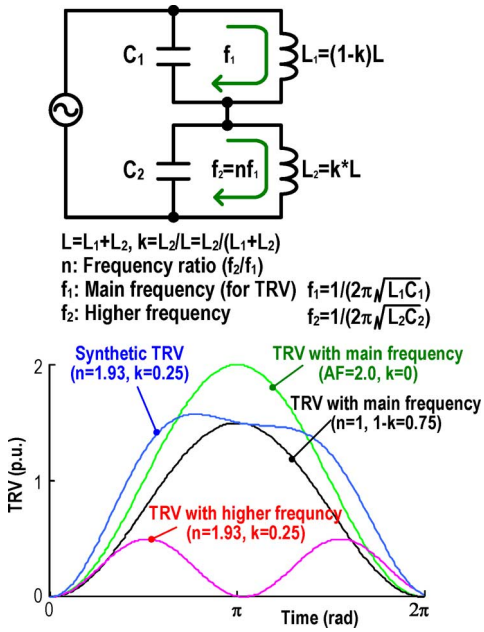

Fig. 17. Synthetic TRV with double frequency components.

V. Effect of the Superimposition of Higher Frequency Components on TRV

The changes of TRV amplitude factor and RRRV due to the superimposition of higher frequency components on TRV were studied with a double-frequency model shown in Fig. 17, where TRV can be represented by the following equation with a main frequency f_1 and a higher frequency f_2:

$$V \approx E \times [(1-k) \times (1-\cos 2\pi f_1 t) + k \times (1-\cos 2\pi f_2 t)]. \quad (30)$$

The parameter k means an amplitude ratio of the higher frequency to the main frequency. Fig. 17 shows the synthetic TRV waveforms in the case of $k = 0.25$ (main frequency f_1: 8.04 kHz, higher frequency f_2: 15.5 kHz, $f_2/f_1 = 1.93$), which corresponds to TRV for the secondary-side TLF condition with the shell-type transformer. Compared with the TRV in the case of the main frequency circuit only ($k = 0$), the synthetic TRV is suppressed, and the amplitude factor is reduced from 2.0 to 1.57 (0.79 times). On the other hand, the RRRV becomes 1.09 times higher.

Fig. 18 shows the dependency of the amplitude factor and RRRV on the frequency ratio of the higher frequency to the main frequency (f_2/f_1) in the case of $k = 0.25$ and 0.125. The amplitude factor becomes a minimum value (about 1.53 for $k = 0.25$) and the RRRV increases by about 10% for $k = 0.25$, when the frequency ratio (f_2/f_1) is 2.

Two measured TRV amplitude factors are plotted in Fig. 18 that shows 1.62 for the primary and 1.40 for the secondary side. Compared with the values for $k = 0.25$, the measured amplitude factors are 20% lower for the primary and 10% for the secondary side. The reductions of the amplitude factor might not be only caused by losses or resistance but also distributed circuit characteristics of the practical transformer described in the next chapter.

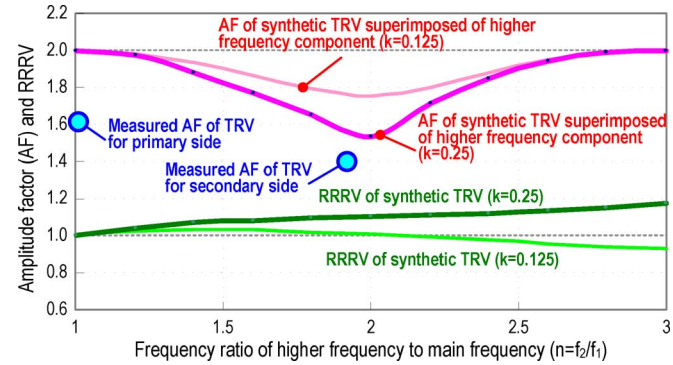

Fig. 18. Dependence of the TRV amplitude factor (AF) and rate of rise of TRV (RRRV) of synthetic TRV on the frequency ratio of a higher frequency component to the main TRV frequency.

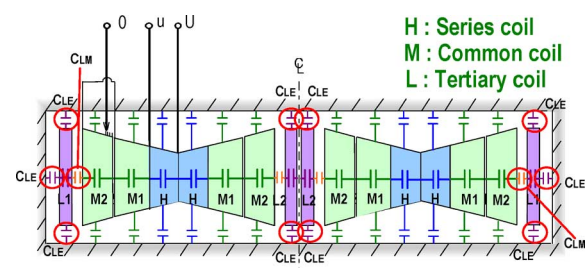

Fig. 19. Cross section of the coil.

VI. TRV Reproduction With Manufacturer Model

In a previous chapter (Section IV), the TRV reproduction using a simplified transformer model based on FRA measurement was evaluated. In this chapter, a precise manufacturer model based on the detailed transformer design is studied and reproduced the TRV waveform using the Electromagnetic Transients Program (EMTP) [8] with this model.

A. Manufacturer Model Based on Transformer Design

Fig. 19 shows the cross-sectional diagram of the transformer coils with two groups used for TRV measurement. The design of the coil is divided into the primary windings (H), secondary windings (M), and tertiary windings (L). Each group has five separate coils consisting of a pair of primary (H) coils, two pairs of secondary (M1 and M2) coils, and two pairs of tertiary (L1 and L2) coils.

Fig. 20 shows an equivalent circuit of the transformers.

The circuits between the primary coil (H) and the secondary coils (M1and M2), between the secondary coils (M1and M2) and the tertiary coils (L1 and L2), and between the primary coil (H) and the tertiary coils (L1 and L2) are modeled with a series-connected resistance and inductance as well as capacitance. The circuits from each terminal to the ground are modeled with the capacitance. The capacitance from the tertiary coil to the ground is expressed as C_{LE}, and that between the tertiary coil and secondary coil is expressed as C_{LM}. These resistances can significantly affect the amplitude of TRV waveforms measured at the power-supply side.

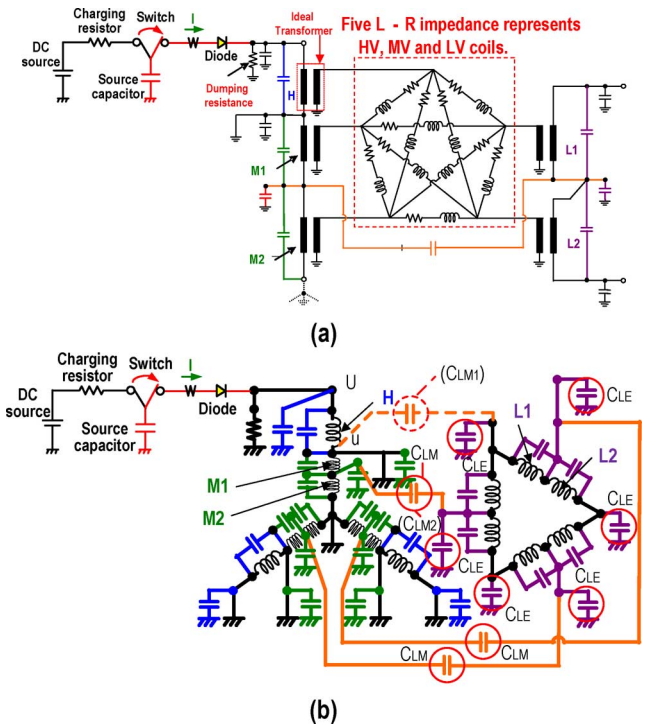

Fig. 20. Five elements model. (a) Single phase transformer model. (b) Three-phase transformer model.

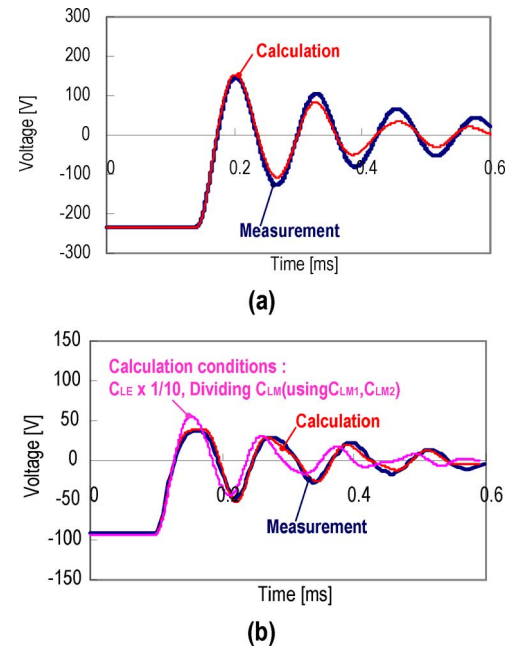

Fig. 21. TRV reproduced by the manufacturer model with five separate coils. (a) Primary side. (b) Secondary side.

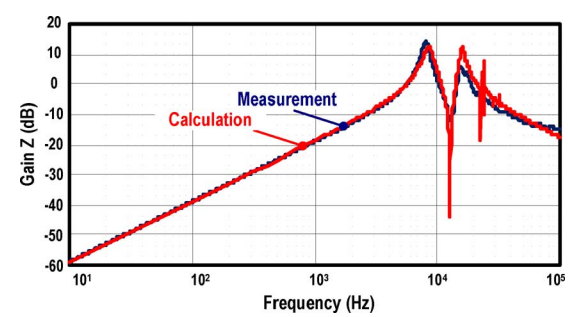

Fig. 22. Response by five elements model (secondary side).

B. TRV Reproduction for the Secondary and Tertiary Side of the Transformer

The TRV for the primary side was calculated with the manufacturer model based on the transformer design and compared with the measured TRV by the capacitor current injection method shown in Figs. 21 and 22. The TRV reproduced by the manufacturer model based on the transformer design shows good agreement with the measurements. The impedance response evaluated with the manufacturer model agreed with the FRA measurement well.

Relatively large capacitance between the tertiary winding and ground (C_{LE}) could be considered as a main contributor for TRV's deformation. TRV was calculated in Fig. 21(b) under the conditions that the capacitance (C_{LE}) is reduced 1/10 in order to confirm the influence on the deformation. The result shows less TRV deformation with reduced capacitance (C_{LE})

In this case, TRV has no deformation. Therefore, TRV's deformation is caused by the capacitance between the tertiary winding and ground.

VII. Conclusion

The TRV phenomena of TLF conditions were investigated and the following results were obtained:

1) TRV waveforms were measured with large capacity shell-type transformers by the capacitor current injection method. Deformation from a sinusoidal shape waveform was observed when the TRV possesses multiple frequency components higher than a main TRV frequency.
2) TRV waveforms were reproduced by the simplified transformer model with a series connection of multiple parallel circuits of L, C, and R evaluated by the FRA measurements depending on the number of the resonant frequency.
3) These equivalent circuit parameters L, C, and R for the simplified transformer model for the primary side deduced with a dumping oscillating response to the step voltage assuming a single frequency by the second Kyoto university method shows good agreements with the values evaluated by the FRA measurement.
4) The TRV amplitude factor is reduced to less than 2.0 due to TRV synthesized with plural frequencies.
5) TRV reproduced by the transformer model based on the design shows good agreement with the measurements by the capacitor current injection method.

This paper will contribute to the future revision of the IEC 62271-100 by explaining the TRV phenomena that can be reproduced by the simplified transformer models based on TRV measurements as well as the manufacturer models with various types of large-capacity power transformers.

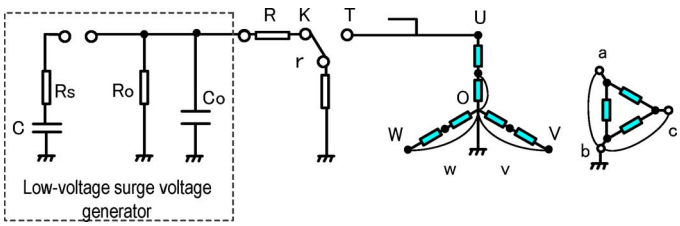

Fig. 23. Measurement of surge impedance (second Kyoto University method).

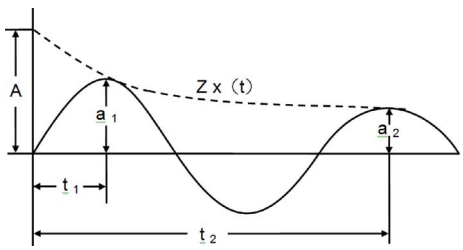

Fig. 24. Waveform of the oscillation appearing between the line terminal and ground.

Appendix
Method of Calculating the Equivalent Circuit Constants of the Transformer According to the Second Kyoto University Method [2]

The second Kyoto university method is a way to measure transient impedance in a power line or electrical equipment by comparing the unknown impedance Z of a power line or electrical equipment to a known high resistance.

Here, the electrical equipment is modeled as a transformer and the unknown impedance Z is represented as a parallel R-L -C circuit to obtain the various constants. The rated transformer tap position is measured with the typical phase for each winding (U phase).

In Fig. 23, switch K connects to r and the generated voltage rises sharply to produce a waveform that has a very long tail, and then the switch connects to T. At that time, a voltage oscillation occurs between the line terminal and ground as shown in Fig. 24.

The oscillation waveform $\mathrm{Zx(t)}$ is expressed by

$$Zx(t) = \mathrm{A} \times \varepsilon^{\alpha \mathrm{t}} \times \sin \omega t. \tag{31}$$

From (31) and Fig. 24

$$a_1 = \mathrm{A} \times \varepsilon^{-\alpha \mathrm{t}1} \tag{32}$$
$$a_2 = \mathrm{A} \times \varepsilon^{-\alpha \mathrm{t}2}. \tag{33}$$

From (32) and (33)

$$\frac{a_2}{a_1} = \varepsilon^{\alpha \times -(\mathrm{t}_2 - \mathrm{t}_1)} \; In \frac{a_2}{a_1} = \alpha \times (t_2 - t_1)$$
$$a = \frac{In \frac{a_2}{a_1}}{t_2 - t_1}. \tag{34}$$

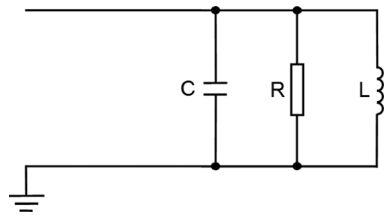

Fig. 25. Transformer lumped constant circuit.

Substituting (34) into (32), A is expressed by

$$A = \mathrm{a}_1 \times \varepsilon \frac{In \frac{a_2}{a_1}}{t_2 - t_1} \times t_1. \tag{35}$$

Further, $\omega = 2\pi f$ and $f = 1/\mathrm{T}$, so from Fig. 24, $\mathrm{T} = t_2 - t_1$. Therefore

$$\omega = 2\pi \frac{1}{t_2 - t_1}. \tag{36}$$

From (34)–(36), α, A, and ω are obtained. Here, the following equation is obtained from converting (31)

$$Z_X(p) = \frac{1}{\frac{1}{A\omega} + \frac{2a}{A\omega} + \frac{a^2 + \omega^2}{A\omega} \times \frac{1}{p}}. \tag{37}$$

The transformer is represented as a lumped constant circuit (Fig. 25). Expressing that circuit as an operator function, the following equation is obtained

$$Z_X(p) = \frac{1}{C \times p + \frac{1}{R} + \frac{1}{L \times p}}. \tag{38}$$

Comparing (37) and (38)

$$C = \frac{1}{A\omega} \; R = \frac{A\omega}{2\alpha} \; L = \frac{A\omega}{\alpha^2 + \omega^2}. \tag{39}$$

Thus, when the transformer is represented as a lumped constant circuit, such as that shown in Fig. 3, the various surge impedance constants can be obtained by using (39).

References

[1] CIGRE Working Group A3.22, "Technical requirements for substation equipment exceeding 800 kV," CIGRE Tech. Brochure 362, 2008.
[2] CIGRE Working Group A3.22, "Background of technical specifications for substation equipment exceeding 800 kV AC," CIGRE Tech. Brochure 456, 2011.
[3] M. Steurer, W. Hribernik, and J. H. Brunke, "Calculating the transient recovery voltage associated with clearing transformer determined faults by means of frequency response analysis," *IEEE Trans. Power Del.*, vol. 19, no. 1, pp. 168–173, Jan. 2004.
[4] W. Hribernik, L. Graber, and J. H. Brunke, "#Inherent transient recovery voltage of power transformers – A model-based determination procedure," *IEEE Trans. Power. Del.*, vol. 21, no. 1, pp. 129–134, Jan. 2006.
[5] R. Horton, R. C. Dugan, K. Wallace, and D. Hallmark, "Improved autotransformer model for transient recovery voltage (TRV) studies," *IEEE Trans. Power Del.*, vol. 27, no. 2, pp. 895–901, Apr. 2012.
[6] M. Steurer, W. Hribernik, and J. H. Brunke, "Calculating the transient recovery voltage associated with clearing transformer determined faults by means of frequency response analysis," *IEEE Trans. Power Del.*, vol. 19, no. 1, p. 168, Jan. 2004.
[7] G. Balzer *et al.*, "Switching of transformer limited faults in HV and EHV systems," in *CIGRE Recife Colloq.*, vol. 77.

[8] H. W. Dommel, *EMTP Theory Book*. Portland, OR, USA: BPA, 1992.

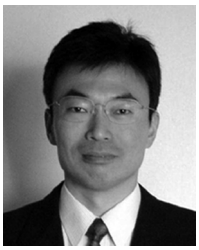

Hiroki Ito (M'11) received the M.S. and Ph.D. degrees in electrical engineering from the Tokyo Institute of Technology Japan, Tokyo, Japan, in 1984 and 1994, respectively.

He joined the Transmission & Distribution Systems Center, Mitsubishi Electric Corporation, Tokyo, in 1984 and was engaged in the research and development of high-voltage dc and ac gas circuit breakers. Currently, he is Senior Chief Engineer of the Energy and Industrial Systems Group. Since 2007, he has been the convener of the CIGRE Working Group A3.22/28 and appointed to be the Chairman of CIGRE Study Committee A3 in 2012.

Hiroki Kajino (M'13) received the B.Eng. and M.Eng. degrees in electrical engineering from Doshisha University, Kyoto, Japan, in 1995 and 1997, respectively.

He joined Mitsubishi Electric Corporation, Tokyo, Japan, in 1997 and is a member of the Engineering Group, T&D Systems Engineering Center, Mitsubishi Electric Corporation. He has been engaged in substation engineering work and the development of substation equipment.

Mr. Kajino is a member of the Institute of Electrical Engineers of Japan.

Yoshibumi Yamagata received the M.S. and Ph.D. degrees in electrical engineering from Yokohama National University, Yokohama, Japan, in 1978 and 2002, respectively.

He joined Tokyo Electric Power Company (TEPCO), Tokyo, Japan, in 1978 and was mainly engaged in the development of bulk power substation equipment such as ultra-high voltage.

Dr. Yamagata is a member of CIGRE, and the Institute of Electrical Engineers of Japan. Since 2012, he has been with Takaoka Electric Manufacturing Company.

Kenji Kamei joined Mitsubishi Electric Corporation, Hyogo, Japan, in 1973. He has taken charge of various developments and their type tests of high-voltage equipment, such as ac and dc circuit breakers, transformers, fuses, and controlled switching devices. Currently, he is a Manager of the R&D Department of the Transmission and Distribution Systems Center, Mitsubishi Electric Corporation.

Mr. Kamei is a member of the Institute of Electrical Engineers of Japan.

Toshiki Idemaru received the B.Eng. and M.Eng. degrees in electrical engineering from Osaka City University, Osaka, Japan, in 1987 and 1989, respectively.

He joined Mitsubishi Electric Corporation, Hyogo, Japan, in 1989, and has been engaged in the research and development of power transformers. Currently, he is Manager of the development section.

Hiromu Shinkai graduated from Seikei University, Tokyo, Japan, in 1974.

He joined Mitsubishi Electric Corporation, Hyogo, Japan. He has been mainly engaged in the design and development of shell-form transformers, such as ultra-high voltage, 500 kV ac and HVDC.